HHS Public Access

Author manuscript

Curr Biol. Author manuscript; available in PMC 2023 March 28.

Published in final edited form as:

Curr Biol. 2022 March 28; 32(6): 1262–1274.e4. doi:10.1016/j.cub.2022.01.040.

ESCRT dysfunction compromises endoplasmic reticulum maturation and autophagosome biogenesis in *Drosophila*

Ruoxi Wang[1,3], **Guangyan Miao**[1], **James Shen**[1], **Tina Fortier**[1], **Eric H. Baehrecke**[1,2,3,*]

[1]Department of Molecular, Cell and Cancer Biology, University of Massachusetts Chan Medical School, Worcester, MA 01605 USA

[2]Lead contact

SUMMARY

Autophagy targets cytoplasmic materials for degradation, and influences cell health. Organelle contact and trafficking systems provide membranes for autophagosome formation, but how different membrane systems are selected for use during autophagy remains unclear. Here we report a novel function of the Endosomal Sorting Complexes Required for Transport (ESCRT) in the regulation of endoplasmic reticulum (ER) coat protein complex II (COPII) vesicle formation that influences autophagy. The ESCRT functions in a pathway upstream of Vps13D to influence COPII vesicle transport, ER-Golgi intermediate compartment (ERGIC) assembly and autophagosome formation. *Atg9* functions downstream of the ESCRT to facilitate ERGIC and autophagosome formation. Interestingly, cells lacking either ESCRT or Vps13D functions exhibit dilated ER structures that are similar to Cranio-Lenticulo-Sutural Dysplasia patient cells with *SEC23A* mutations, which encodes a component of COPII vesicles. Our data reveal a novel ESCRT-dependent pathway that influences the ERGIC and autophagosome formation.

Graphical Abstract

[*]Correspondence to: Eric H. Baehrecke, Department of Molecular, Cell, and Cancer Biology, 423 Lazare Research Building, 364 Plantation St., University of Massachusetts Chan Medical School, Worcester, MA 01605, USA. Telephone: +1-508-856-6733, eric.baehrecke@umassmed.edu.

[3]Twitter: @BaehreckeLab (E.H.B.), @Ruoxi52101264 (R.W.)

AUTHOR CONTRIBUTIONS

R.W. and E.H.B. designed experiments, R.W., G.M., J.L.S., and T.M.F. performed experiments, R.W. and E.H.B. wrote the manuscript and all authors commented on it.

DECLARATION OF INTERESTS

EHB is a member of the Advisory Board of Current Biology. All other authors declare no competing interests.

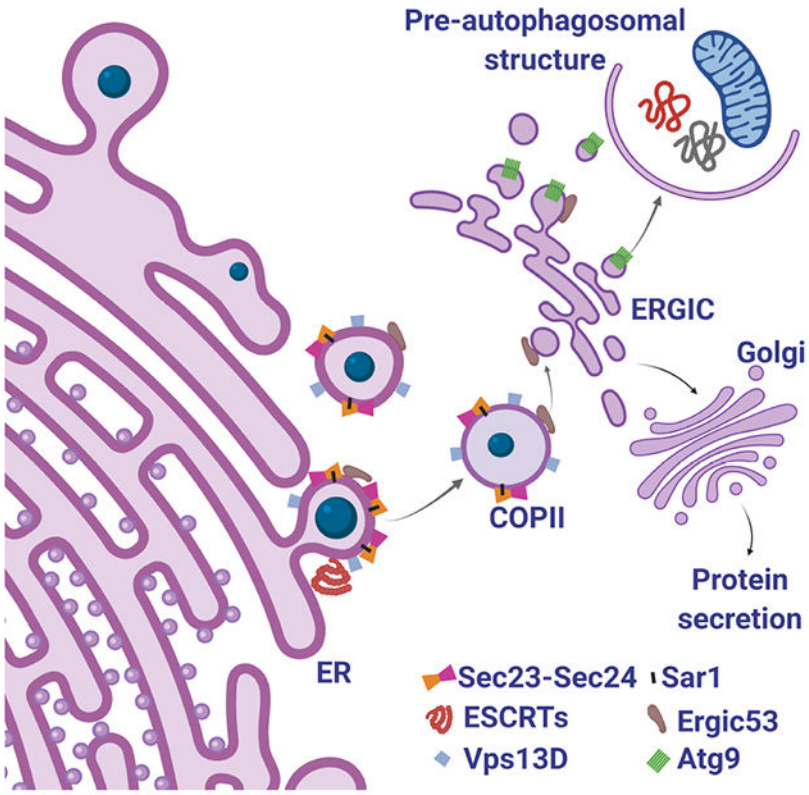

eTOC blurb

The removal of cytoplasmic materials by autophagy is important for cell and organism health. Wang et al. identify a relationship between the Endosomal Sorting Complexes Required for Transport (ESCRT) and Vps13D in the regulation of endoplasmic reticulum (ER) coat protein complex II (COPII) vesicle formation that influences autophagy.

Keywords

ESCRT; VPS13D; Atg9; autophagy; *Drosophila*

INTRODUCTION

Components of the coat protein complex II (COPII) are responsible for the formation of endoplasmic reticulum (ER)-derived vesicles and transport toward the Golgi apparatus [1]. COPII vesicles are an important source of membrane for the assembly of the ER-Golgi intermediate compartment (ERGIC)[2] and the protein secretory pathway [1]. COPII coat formation is initiated by the small GTPase Sar1 (Secretion associated, ras-related) which recruits the COPII inner coat Sec23-Sec24 and outer coat Sec13-Sec31 protein complexes [1]. Interestingly, *SEC23A* has been implicated in the rare genetic disease cranio-lenticulo-sutural dysplasia (CLSD) [3]. *SEC23A* F382L mutation leads to a defect in the recruitment of COPII proteins and dilated ER with multiple tubular projections on the ER surface [1].

Macroautophagy (autophagy) delivers cytoplasmic cargoes to the lysosome to reduce stress and modulate cellular homeostasis [4]. Autophagic cargoes, including damaged organelles, protein aggregates, pathogens and macromolecules, are sequestered in double-membrane autophagosomes that fuse with lysosomes for degradation. Bulk autophagy can be initiated by nutrient deprivation that involves the class I PI3-kinase and mTOR nutrient sensing pathways [5, 6]. Inactivated mTOR releases the inhibition of the Atg1 complex and initiates autophagy that requires activation of the Vps34 complex (PI3KC3-C1 in mammals) [7].

The ER is an important membrane source for autophagosomes [8]. ER provides membrane from contact with mitochondria to facilitate autophagosome membrane nucleation [9]. Both COPII ER components and Atg9 are important regulators of autophagosome membrane formation [10–15]. The ER-dependent ERGIC membrane compartment is required for LC3 (Atg8 in lower organisms) lipidation [16, 17]. Atg9 interacts with Sec24 [18], these proteins are localized near mitochondria and the Golgi apparatus [8], and are enriched in the same biochemical fractions with the ERGIC in mammalian cells [16]. In yeast, COPII vesicles facilitate the recruitment of autophagy proteins, including Atg8 and Atg9, to phagophore assembly sites [19]. In addition, Sec24 interacts with an ER-phagy receptor to modulate ER quality control [20].

Autophagy is regulated in a context-specific manner during both development and disease [4, 21]. During *Drosophila* development, autophagy in intestine cells requires the function of many core autophagy (*Atg*) genes, but does not require either the E1-like *Atg7* or E2-like *Atg3* genes [22]. By contrast, the ubiquitin activating enzyme *Uba1*-encoding gene is required for autophagy-dependent cell size reduction [22]. In addition, the putative ubiquitin-binding-domain encoding genes *Vps13D, Tsg101*, and *Vps36* were identified in a screen for factors that are required for autophagosome formation and cell size reduction in intestines [23]. Vps13D regulates mitochondria and ER contact, autophagosome formation and is recruited to the ER to transfer lipids to mitochondria [23–25]. Tsg101 and Vps36 are essential components of the ESCRT which is known to regulate autophagosome and lysosome fusion, as well as autophagosome membrane sealing [26–28].

The ESCRT has multiple functions in divergent vesicle formation and membrane trafficking events within cells [29]. Here we show that multiple ESCRT component-encoding genes are required for autophagy and intestine cell size reduction. ESCRT components function upstream of *Vps13D*, and influence COPII and ERGIC proteins to modulate COPII vesicle formation and ER morphology. In addition, ESCRTs and Vps13D regulate COPII-dependent ERGIC assembly to influence Atg9 distribution and modulate autophagosome formation. These studies reveal a novel ESCRT-dependent mechanism for the formation of COPII vesicles that are used to form autophagosomes through the functions of Vps13D and Atg9.

RESULTS

The ESCRT and Vps13D function in a common pathway to regulate autophagy

A screen was conducted for genes encoding putative ubiquitin binding domains that influence developmental autophagy in the *Drosophila* larval intestine [23]. Through this screen, multiple regulators of autophagy were identified, including *Vps13D, Tsg101* and

Vps36 [23]. Tsg101 and Vps36 are components of the ESCRT, and the ESCRT is required for autophagosome and lysosome fusion in the *Drosophila* fat body [30]. Therefore, we investigated the function of ESCRT-encoding genes in larval intestine cells to determine if they have a similar function in autophagosome and lysosome fusion. In contrast to fat body cells, Hrs^{D28} (ESCRT-0), $Vps25^{N55}$ (ESCRT-II), and $Vps32^{G5}$ (ESCRT-III) loss-of-function mutant intestine cells fail to form mCherry-Atg8a autophagy reporter puncta 2 hours after puparium formation (APF) while neighboring control cells form robust mCherry-Atg8a puncta (Figures 1A and 1B; Figures S1A–S1D). Similarly, Atg8a lipidation is decreased in *Vps25* and *Vps36* knockdown intestine cells (Figures 1C and 1D). In addition, the autophagic receptor and substrate Ref2p accumulated in *Vps25* and *Vps36* knockdown cells, as well as in Hrs^{D28}, $Vps25^{N55}$, and $Vps32^{G5}$ mutant cells, compared to control intestine cells (Figures 1C, 1F–1G; Figures S1E–S1H). Importantly, autophagosome and autolysosome structures are significantly decreased in *Vps25* and *Vps36* knockdown intestine cells based on transmission electron microscope (TEM) analyses (Figures 1H–1K). Furthermore, the regulator of autophagosome and lysosome fusion Syntaxin17 is decreased in $Vps25^{A3}$ loss-of-function mutant cells compared to neighboring control cells (Figures 1L and 1M). These results are in contrast to what was previously described in cells of the fat body of feeding third larval instar *Drosophila* [30], where loss of either Hrs^{D28}, $Vps25^{N55}$ or $Vps32^{G5}$ mutant cells possess an increase in the number of mCherry-Atg8a autophagy reporter puncta (Figures S1I–S1N). The combined inhibition of mCherry-Atg8a reporter puncta formation, accumulation of Ref2p, and reduction in autophagic structures indicate that ESCRT-encoding genes are required for autophagy initiation during larval intestine development.

Autophagy is used to clear mitochondria by mitophagy in intestine cells [22]. Therefore, we next asked if mitochondrial cargoes fail to be cleared in ESCRT mutant intestine cells. Indeed, cells lacking either $Vps25^{N55}$ or $Vps32^{G5}$ failed to clear the mitochondrial protein ATP5a, a surrogate marker of mitochondria, while control neighboring cells lacked ATP5a (Figures 1N and 1O; Figures S1O–R). Combined, these data indicate that ESCRT-encoding genes are required for the initiation of autophagy and therefore clearance of cytoplasmic cargoes, including mitochondria.

Intestine cells lacking the function of ESCRT encoding genes possess similar phenotypes to *Vps13D* mutant cells. To test if the ESCRT and Vps13D may function in the same pathway, we analyzed Vps13D protein puncta in ESCRT gene mutant intestine cells. While control cells possess numerous Vps13D puncta in intestine cells 2 hours APF when autophagy is induced, neither *Vps25* nor *Vps32* mutant cells possess similar Vps13D puncta (Figures 2A–2D). These data suggest that Vps13D functions downstream of the ESCRT to regulate intestine cell autophagy.

We next tested if the ESCRT and Vps13D function in the same or parallel genetic pathways. We analyzed Ref2p in $Vps13D^{MI}$ loss-of-function mutant cell clones in either luciferase control RNAi, *Vps25* RNAi or *Vps36* RNAi knockdown intestines to determine if the ESCRT and Vps13D have either additive or the same phenotypes, thus indicating if they are in parallel or the same genetic pathway. Importantly, knockdown of either *Vps25* or *Vps36* function by expression of RNAi failed to enhance the number of Ref2p puncta in $Vp13D^{MI}$

mutant cells (Figures 2E–2H; Figures S1S–S1U). Combined, these results indicate that the ESCRT functions upstream of Vps13D in a common pathway to regulate autophagy.

The ESCRT influences the COPII pathway

The relationship between the ESCRT and Vps13D prompted us to consider where these proteins are localized and therefore how they may influence autophagy. While Hrs was diffuse with some punctate localization in intestine cells during the third instar larval stage, Hrs puncta co-localized with the ER-associated Sec61α protein marker and the ER-exit-site (ERES) protein Sec16 marker at pupation when autophagy is induced (Figures S2A–S2F). Similarly, Vps13D was not associated with markers of organelles in intestine cells during the third larval instar [23], but Vps13D was juxtaposed to the Golgi-associated GalT marker at pupation when autophagy is induced (Figures S2G–S2I). These results indicate that Hrs and Vps13D are localized near the ER and Golgi apparatus, respectively, at the developmental stage when autophagy is induced in intestine cells.

The association of Hrs and Vps13D near the ER and Golgi apparatus prompted us to consider the localization of markers of COPII vesicles and the ERGIC, the compartments of transport between ER and the Golgi apparatus [2]. Sec23 is a component of the COPII coat and transports to the ERGIC [1]. At third larval stage, Sec23 was mostly localized near the ER marker Sec61α (Figure S2J), and then dissociated from the ER membrane at pupation (Figures S2K and S2L). In addition, the ERGIC component Ergic53 [31] was co-localized with Sec23 at the third larval stage (Figure S2M), and this co-localization increased significantly at pupation (Figures S2N and S2O). These data suggest that Ergic53 is transported with the COPII protein Sec23 between ER and the Golgi apparatus when autophagy is activated at pupation.

We next tested if changes in the COPII-associated secretory pathway require the ESCRT during autophagy. Both Sec23 and Sec61α puncta were co-localized in $Vps25^{A3}$ mutant third larval instar intestine cells (Figures S2P and S2Q). Similarly, both Sec23 and Ergic53 puncta were co-localized in $Vps25^{A3}$ mutant intestine cells at the same stage (Figures S2R and S2S). While Sec16 puncta appeared to be similar in $Vps25^{A3}$ loss-of-function mutant and control intestine cells 2 hours APF, Sec23 was reduced and significantly less associated with Sec16 in $Vps25^{A3}$ mutant cells (Figure 3A and 3B). Similarly, Sec23 and Ergic53 were decreased and dissociated in $Vps25^{A3}$ loss-of-function mutant intestine cells compared to control neighboring cells 2 hours APF (Figures 3C and 3D). These data indicate COPII vesicle markers require the ESCRT in a stage-specific manner that coincides with the activation of autophagy. In addition, Hrs was partially localized with Ergic53 in control neighboring intestine cells 2 hours APF (Figures 3E and 3F), but Hrs puncta were increased and enlarged with decreased Ergic53 association in $Vps25^{A3}$ mutant intestine cells (Figures 3E and 3F).

A rise in the steroid hormone ecdysone is the primary trigger of autophagy in the fly larval intestine [22]. By contrast, the fat body is a nutrient sensing organ that undergoes starvation-triggered autophagy in *Drosophila* [5]. Therefore, we next tested the influence of starvation on Sec16, COPII and ERGIC markers in the fat body. Sec16 puncta formation was not influenced by loss of *Vps25* compared to neighboring control cells in the fat body of

starved larvae (Figure S3A). Additionally, Sec16 and Sec23 co-localization was comparable in *Vps25* mutant compared to control neighboring fat body cells (Figure S3A and S3B). Importantly, Sec23 and Ergic53 co-localization was not significantly different between in *Vps25* mutant and neighboring control cells in the fat body cells of feeding animals (Figure S3C and S3E). However, fat body cells from starved animals exhibit increased Ergic53 puncta size, and these larger puncta are not co-localized with Sec23 (Figure S3D and S3E). In addition, *Vps25* mutant fat body cells from starved larvae possess significantly decreased Ergic53 puncta compared to control cells (Figure S3D and S3E). Sec23 and Sec22 co-localization was not significantly different between *Vps25* mutant and neighboring control fat body cells in feeding animals (Figure S3F and S3H). Additionally, Sec22 puncta size was increased in the control fat body cells from starved larvae, while Sec22 puncta appeared to be smaller in *Vps25* mutant than in control fat body cells (Figure S3G and S3H). Interestingly, *Vps25* does not influence Sec22 puncta co-localization with Sec23 in fat body cells from animals under nutrient restriction conditions (Figure S3G and S3H). Combined, our data suggest nutrient restriction conditions that are known to regulate autophagy also impact how Vps25 influences the ERGIC in the *Drosophila* fat body.

The ESCRT has been implicated in multiple membrane remodeling processes [32]. However, our data are inconsistent with the ESCRT functioning in the control of known membrane fusion events during autophagy in larval intestine cells. Considering the ESCRT's function in the regulation of endosome maturation [30], we next investigated the role of the ESCRT in intestine cell endocytosis. *Vps34* (class III PI3K) is a known regulator of both autophagy and endocytosis [33]. *Vps34* loss-of-function mutant intestine cells possess decreased ESCRT protein-Hrs puncta (Figures S4A and S4B). In addition, *Vps34* mutant intestine cells possess decreased fluid phase uptake of TR-avidin by endocytosis compared to neighboring control cells (Figures S4C and S4F). In contrast to *Vps34* mutant cells, $Vps25^{A3}$ mutant cells accumulate TR-avidin puncta (Figures S4D and S4F), and $Vps34^{m22}$ $Vps25^{A3}$ double mutant cells possess decreased TR-avidin puncta (Figures S4E and S4F). Importantly, *Vps34* and *Vps25* both influence the late endosome marker Rab7 (Figures S4G–S4I), and lysosomal enzyme Cathepsin B activity (Figures S4J–S4L). Combined, these data suggest that Vps34 and the ESCRT regulate endocytosis at different stages in the same pathway. Therefore, we next tested if Vps34 influences COPII trafficking through the endocytosis system. In contrast to the influence of *Vps25* on Sec23 and Ergic53 puncta distribution (Figures 3G and 3J), *Vps34* loss failed to influence Sec23 and Ergic53 co-localization (Figures 3H and 3J). Importantly, loss of both *Vps25* and *Vps34* in double mutant cells have the same phenotype as *Vps25* single mutant cells (Figures 3I and 3J). Combined, these data indicate that the ESCRT regulates COPII and ERGIC puncta formation in a manner that is independent of Vps34 function.

The secretory pathway not only regulates membrane exchange between ER and the Golgi apparatus, but also influences ER morphology [1]. Cranio-Lenticulo-Sutural Dysplasia (CLSD) patient cells with mutations in *SEC23A* exhibit dilated ER with multiple tubular projections on the ER surface due to defects of COPII coat formation [1]. Interestingly, *Vps25* and *Vps36* knockdown intestine cells exhibit dilated ER based on TEM analyses (Figures 3K–3M). These ER structures are similar to the ER morphology observed in *SEC23A* mutant CLSD patient cells, with some of the tubular structures being variable in

morphology. These data indicate the ESCRT regulates COPII vesicle formation, and that like COPII components, the ESCRT is required for proper ER structure.

Vps13D, COPII and the ERGIC function in a common autophagy pathway

We investigated the localization of Vps13D with markers of COPII and the ERGIC, and how altered *ESCRT* function influences their localization. Interestingly, Vps13D was co-localized with Ergic53 in control intestine cells 2 hours APF (Figures 4A and 4B, inset "Ctrl"), but dissociated from Ergic53 in $Vps25^{A3}$ mutant intestine cells (Figures 4A and 4B, inset A3). Furthermore, Vps13D and Sec23 were partially co-localized in control intestine cells 2 hours APF, but dissociated in $Vps25^{N55}$ mutant intestine cells (Figures 4C and 4D). Consistent with these data, the ERGIC component Sec22 associated with Vps13D in control intestine cells 2 hours APF, but Sec22 puncta were smaller and dissociated from Vps13D puncta in $Vps25^{A3}$ mutant cells (Figures S5A–S5C). In addition, Sec22 co-localized with the *cis*-Golgi protein GM130 in control intestine cells 2 hours APF, but Sec22 and GM130 were less associated in $Vps25^{A3}$ mutant intestine cells (Figures S5D and S5E). Combined, these data indicate that the ESCRT is required for Vps13D localization with markers of ER, the ERGIC and Golgi.

The co-localization of Vps13D with markers of COPII vesicles prompted us to test whether loss of *Vps13D* influences COPII-associated proteins. Consistent with an impact on trafficking, Sec23 puncta were decreased in *Vps13D (MiMIC)* loss-of-function mutant cells compared to control cells 2 hours APF (Figures 4E and 4F). We also analyzed Sec23 and Ergic53 in *Vps13D* (*ΔUBA*) (UBA domain deleted)/*Df*(*3L*)*BSC613* (*ΔUBA/Df*) mutant intestine cells. Sec23 and Egic53 puncta were decreased, smaller, and had less co-localization in *Vps13D* (*ΔUBA/Df*) intestine cells compared to the control intestine cells (Figures 4G–4J). In addition, Sec22 and Sec23 structures were disorganized and had smaller puncta in *Vps13D* (*ΔUBA/Df*) mutant intestine cells (Figures S5F–S5I).

Our results indicate that the ESCRT and Vps13D both influence markers of COPII vesicle formation. Therefore, we investigated if *Vps13D* influences ER morphology as observed with ESCRT loss. Indeed, Sec61α structures were disorganized and formed large puncta in *Vps13D* (*ΔUBA/Df*) mutant intestine cells (Figures S5J–S5L), similar to the ER structures in CLSD patient cells [1]. Significantly, TEM analyses revealed dilated ER with multiple tubular projections on the ER surface in *Vps13D* (*ΔUBA/ Df*) intestine cells (Figures 4K–4L). Although some of the tubular structures are variable in morphology, they are similar to what was observed in intestine cells with reduced *Vps25* and *Vps36* function (Figures 3K–3M). Combined, our results indicate that *Vps13D* functions in same pathway with the ESCRT to impact markers of COPII vesicle trafficking from the ER to influence the ERGIC.

The ER is a membrane source for COPII vesicles, the ERGIC and autophagosomes [34]. Thus, we investigated the relationship between the autophagy protein Atg8a and ER-derived vesicles prior to and during autophagy initiation. Prior to the activation of autophagy in third larval stage intestines, Atg8a was more diffuse and less associated with the ER, ERES and ERGIC protein markers Sec61α, Sec16 and Ergic53 (Figures 5A, 5D and 5G). By contrast, Atg8a puncta were increased and partially co-localized with Sec61α and Sec16,

and juxtaposed with Ergic53, puncta when autophagy was activated in intestine cells after puparium formation (Figures 5A–5I).

The ERGIC facilitates the formation of autophagosome membrane precursors [16]. Therefore, we investigated the relationship between genes known to be required for ERGIC assembly and autophagy in intestine cells. Importantly, mCherry-Atg8a puncta were significantly decreased in *Sec22* RNAi-expressing intestine cells compared to neighboring control cells (Figures 6A and 6B). In addition, *Sec22* knockdown cells possess increased autophagy cargo receptor Rep2p/p62 (Figures 6C and 6D). Sar1 recruits and activates COPII coats [2], and facilitates ERGIC assembly [16]. Importantly, *Vps25* mutant intestine cells possess increased Sar1 puncta (Figures 6E and 6F). In addition, Re2p/p62 puncta were increased in *Sar1* mutant intestine cells compared to neighboring control cells (Figures 6G and 6H). In addition, Vps13D puncta were decreased while Sec23 puncta were increased in *Sar1* mutant intestine cells, and the co-localization of Vps13D with Sec23 was decreased in these mutant intestine cells (Figures 6I–6K). Combined, these results indicate that ER-derived vesicles are required for Vps13D recruitment to facilitate autophagosome formation.

The ESCRT influences Vps13D, COPII, ERGIC and Atg9 to impact autophagy

Atg9 is an important regulator of autophagosome formation that interacts with multiple membrane sources [35–37]. Consistent with previous work in other cells and organisms, mCherry-Atg8a reporter puncta were significantly decreased in $Atg9^{D51}$ loss-of-function mutant compared to neighboring control intestine cells (Figures 7A and 7B). In addition, autophagy cargo receptor Ref2p/p62 puncta were increased in $Atg9^{D51}$ mutant compared to control intestine cells (Figures 7C and 7D).

Atg9 interacts with COPII vesicles for autophagy induction in yeast [18]. Therefore, we investigated the relationship between Atg9 and COPII vesicle components. Sec23 and Ergic53 puncta were both elongated and co-localized with each other in *Atg9* mutant compared to neighboring control intestine cells (Figures 7E–7E”). Similarly, the ERES component Sec16 and Sec23 were co-localized in *Atg9* mutant intestine cells (Figure S6A–A”), Interestingly, Ergic53 was juxtaposed to the *cis*-Golgi protein GM130 in *Atg9* mutant intestine cells at puparium formation (Figures S6B–S6B”). Additionally, Sec22 localization with GM130 was similar in *Atg9* mutant and neighboring control cells (Figures S6C–S6C”). Combined, these data indicate that COPII vesicle components and the ERGIC membrane either accumulate or are remodeled when autophagy is impaired.

We next investigated the relationship between the ESCRT and Atg9 with markers of COPII trafficking that are associated with autophagy. Interestingly, Atg9 is observed throughout the cytoplasm and adjacent to Ergic53 puncta in control cells, while *Vps25* mutant cells possess fewer Ergic53 puncta (Figure S6D). Significantly, both Sec23 and Ergic53 puncta were decreased and dissociated in $Vps25^{N55}$ $Atg9^{D51}$ double mutant intestine cells (Figures 7F–7F”). These data suggest that the ESCRT is required for Atg9 to stabilize the localization of Sec23 and Ergic53. In addition, both Vps13D and Ergic53 puncta were elongated and co-localized in *Atg9* mutant intestine cells (Figures 7G–7G”). By contrast, Sec22 puncta were juxtaposed with Vps13D in *Atg9* mutant intestine cells compared to the neighboring control cells at puparium formation (Figures S6E–S6E”). Importantly, the co-localization of

Vps13D and Ergic53 puncta was decreased in *Vps25*^{N55} *Atg9*^{D51} double mutant intestine cells (Figures 7H–7H"). These data suggest that the ESCRT is required for Atg9 to stabilize the co-localization of Vps13D and Ergic53. Combined, these data indicate that the ESCRT influences Vps13D function to regulate the COPII and ERGIC to modulate autophagy that depends on Atg9.

DISCUSSION

The ESCRT regulates autophagy in multiple ways, including autophagosome membrane sealing and autolysosome formation [27, 28, 38]. This study reveals a previously undescribed function of the ESCRT in ER trafficking and autophagy. Our findings indicate that the ESCRT is required for COPII vesicle-derived compartments and autophagosome formation. Loss of ESCRT components influence COPII vesicle marker formation and ER morphology. We also show that Vps13D co-localizes with markers of different stages of COPII vesicle maturation between the ER and Golgi apparatus, including markers of ERGIC formation. In the absence of ESCRT and Vps13D function, ER structure is altered in a manner that is similar to Cranio-Lenticulo-Sutural Dysplasia patient cells with *SEC23A* mutations [1]. In addition, the ESCRT impacts Atg9 distribution. Vps13D and Atg9 are required for autophagy, and appear to influence the ERGIC for the induction of autophagy. Therefore, this study identifies previously unrecognized steps in a regulatory pathway for autophagy, including novel roles for the ESCRT and Vps13D in COPII-derived and ERGIC-associated autophagosome formation.

Autophagy involves a core mechanism [4], but some autophagy regulatory mechanisms vary in different cell-contexts in animals [21]. During *Drosophila* midgut development, most of the core autophagy genes are required, but *Atg7* and *Atg3* are not required for cell size reduction, protein and organelle clearance [22]. Instead, the ubiquitin activating enzyme Uba1 and ubiquitin function in autophagy. Vps13D contains a conserved ubiquitin binding UBA domain and is required for developmental autophagy in the fly intestine. Thus, Vps13D has properties of an autophagy receptor [23], and therefore may link ubiquitin, autophagy proteins, and their autophagic cargo substrates. Alternatively, ubiquitin may have cargo receptor-independent functions in autophagy during intestine development.

Tsg101 and Vps36 both possess ubiquitin binding domains and are required for autophagy in the fly intestine [23]. While previous studies have shown that the ESCRT functions in autophagosome membrane sealing and autolysosome formation [27, 28, 38], our studies of *Tsg101, Vps36* and all other ESCRT components tested indicate a novel role in ER trafficking for autophagosome formation in the intestine. We systematically compared ESCRT function in different cell contexts in *Drosophila.* Consistent with previous studies [30], *ESCRT* mutant fat body cells accumulate Atg8a puncta indicating that autophagy is blocked following autolysosome formation. By contrast, the ESCRT is required for Atg8a puncta formation in intestine cells. Therefore, the ESCRT machinery functions in a cell context-specific manner to regulate autophagy.

ESCRT machinery regulates multiple dynamic membrane changes, including vesicle abscission, membrane sealing and repair [29, 39]. The function of the ESCRT in the COPII

pathway is novel, but also has similarities to the essential function of the ESCRT in membrane remodeling. During *Drosophila* development, Hrs is distributed near ER and co-localized with Ergic53 when autophagy is induced. In *ESCRT* mutant cells, both COPII and Ergic53 puncta were decreased and dissociated, indicating COPII vesicles derived from ER are inhibited without the ESCRT. Multiple membrane remodeling processes require the ESCRT, including vesicle budding and internalization. Thus, it appears that the ESCRT affects COPII coated ER exit sites to shed vesicles and influences ERGIC and autophagosome assembly in a cell-specific manner. Decreased function of ESCRT regulatory genes influences Vps13D levels. By contrast, Vps13D regulates COPII regulatory protein localization, suggesting that Vps13D functions downstream of the ESCRT to influence COPII. It should be noted, however, that it is difficult to exclude the possibility that the ESCRT may also participate in either autophagosome membrane sealing or fusion between autophagosome and lysosome at a later stage in the autophagy process. In addition, we cannot exclude possible an indirect influence of the ESCRT on the ER and COPII maturation that is independent of Vps34.

The roles of regulators of COPII vesicle and ERGIC formation in autophagy may be *Drosophila* intestine cell context-specific. However, COPII and the ERGIC have been implicated in the regulation of autophagy in both yeast and mammalian cells. Atg9 interacts with membrane compartments from the secretory pathway, endocytic vesicles and Golgi apparatus in both yeast and mammals [40]. Atg9 interacts with the COPII component Sec24 in yeast, and co-fractionates with ERGIC components in mammalian cells [16, 18]. Thus, it is likely that membranes from COPII compartments are utilized for autophagy induction. *Atg9* is conserved in *Drosophila*, and our analyses indicate that *Atg9* is downstream of the ESCRT, Vps13D and the ERGIC. Therefore, the ERGIC is also a potential membrane source for Atg9 to regulate the induction of autophagy in *Drosophila*, consistent with ERGIC function in mammalian cells [16]. Thus, it is possible that the roles of COPII, Vps13D and the ERGIC are more prevalent in the regulation of autophagy than previously recognized. Future studies should reveal how broadly these factors function in autophagy, as well as the role of the ESCRT in COPII vesicle maturation in other cell types.

STAR★METHODS

RESOURCE AVAILABILITY

Lead contact—Please contact the Lead Contact, Dr. Eric Baehrecke, for additional information and requests for resources and reagents (eric.baehrecke@umassmed.edu).

Materials availability—All unique/stable reagents generated in this study are available from the Lead Contact with a completed Materials Transfer Agreement.

Data and code availability

- Original western blot images have been deposited at Mendeley and are publicly available as of the date of publication. The DOI is listed in the key resources table. Microscopy data reported in this paper will be shared by the lead contact upon request.

- No code was generated in this study.
- Any additional information required to reanalyze the data reported in this paper is available from the lead contact upon request.

EXPERIMENTAL MODEL AND SUBJECT DETAILS

Drosophila melanogaster strains used in this study are listed in the Key resources table. All flies were reared at 25°C on standard cornmeal/molasses/agar media.

METHOD DETAILS

Fly stocks—Flies were reared at 25°C on standard cornmeal-molasses-agar media. For Hrs^{D28} mutant cell clones we crossed *y w hsFlp; Ubi-nlsGFP* virgin females to Hrs^{D28}, *FRT40A/CyO (tb), tb* males. For $Vps25^{N55}$, $Vps25^{A3}$, $Vps32^{G5}$ and $Atg9^{D51}$ mutant clones, we crossed y w hsFlp; FRT42D, Ubi-nlsGFP/RFP to either *FRT42D,* $Vps25^{N55}$*/CyO (tb), FRT42D,* $Vps25^{A3}$*/CyO (tb), FRT42D,* $Vps32^{G5}$*/CyO (tb)*, or *FRT42D,* $Atg9^{D51}$*/CyO (tb).* For $Sar1^{11\text{-}3\text{-}63}$ mutant clones, we crossed *y w hsFlp;;FRT82B, Ubi-nlsRFP* to *FRT82B,* $Sar1^{11\text{-}3\text{-}63}$*/TM6B (tb).* For *Vps13D* clones, we crossed *y w hsFlp;;Ubi-nlsGFP,FRT2A* to $Vps13D^{MI11101}$*, FRT2A/TM6B (tb).* Sar1-GFP line was generated by BestGene Inc. We thank the following researchers for mutant flies: Andreas Bergmann for $Vps25^{N55}$, Guang-Chao Chen for $Atg9^{d51}$ [41] and Thomas P. Neufeld for $Vps34^{m22}$.

Induction of cell clones and quantitation—Loss-of-function mutant cell clones in midgut and fat body were induced as previously described [22, 23]. Adult flies were mated on low yeast food for 4 hours at room temperature, and eggs were collected and heat shocked at 37°C for 1 or 2 hours. To induce RNAi cell clones in midguts, virgin females of *y w hsFlp; mCherry-Atg8a; Act>CD2>GAL4, UAS-nlsGFP* flies were crossed with RNAi lines. One-day-old eggs were heat shocked at 37°C for 15 minutes. For fat body experiments, feeding 3rd instar larvae were dissected. For 3rd instar larval midgut experiments, animals were dissected at 72 hours. For staged midgut experiments, white prepupae were placed on wet filter paper for 2 hours before dissection. All puncta and cell sizes were quantitated as previously described [23].

Immunoblotting—Fly intestines two hours after puparium formation were dissected in prechilled PBS and homogenized in 2xLaemli sample buffer with protease inhibitor cocktail. Homogenates were analyzed by western blot and immunoblotted with anti-Atg8a (1:1000, Cell Signaling Technologies, 13733), anti-Ref2p (1:1000, Gabor Juhasz or Abcam, AB178440) and anti-Actin (1:2000, Developmental Studies Hybdridoma Bank, JLA20) antibodies.

Transmission electron Microscopy—Intestines were dissected in PBS 2 hours after pupation, fixed in a solution of 2.5% glutaraldehyde and 2% paraformaldehyde in 0.1 M sodium cacodylate buffer, pH 7.4 for 1 hour at room temperature, and washed in distilled water. Preparations were stained en bloc in 1% aqueous uranyl acetate for 1 hour at 4°C in the dark, washed in distilled water, dehydrated through a graded ethanol series, treated with propylene oxide and infiltrated in SIP-pon/Araldite for embedding. Ultrathin sections were cut on a Leica UC7 microtome. Sections of the anterior region of the midgut were collected

to ensure an unbiased approach, and stained with uranyl acetate. For each genotype, at least 3 intestines were embedded and sectioned for analyses and quantification. We reviewed all images and selected representative images for analyses. Imaging was performed using a Phillips CM10 TEM.

Immunolabeling and microscopy—Midguts were dissected in PBS, fixed with 4% paraformaldehyde (PFA) in PBS 0.3% Triton X-100 (PBST), and blocked with goat serum for 2 hours before incubating with primary antibodies in 0.3% PBST with 5% goat serum. For Atg8a staining, midguts were dissected in PBS, fixed with heptane and 4% PFA mixture for 20 minutes and then rinsed with methanol 5 times before blocking with 5% goat serum in 0.3% PBST. For immunostaining, we used mouse anti-Vps13D (1:50, [23]), rat anti-Syntaxin 17 (1:400, Gabor Juhasz) rabbit anti-Ref2p/p62 (1:1000, Gabor Juhasz or Abcam, AB178440), mouse anti-ATP5A (1:200, Abcam, Ab14748), pig anti-Hrs (1:600, Hugo J. Bellen), rabbit anti-Atg8a (1:200, Cell Signaling Technologies, 13733), rabbit anti-Sec23 (1:200, Thermo Fisher Scientific, PA1-069A), rabbit anti-GM130 (1:200, Abcam, AB30637), rabbit anti-Atg9A (1:200, Novus Biologicals, NB110-56893SS) antibodies. We used Hoechst dye (Invitrogen, 33342) to stain DNA and the following secondary antibodies (1:200): anti-mouse Alexa Fluor 488 (A-11029), anti-rabbit Alexa Fluor 488 (A-27034), anti-rabbit Alexa Fluor 546 (A-11035), anti-mouse Alexa Fluor 546 (A-11030), anti-guinea pig Alexa Fluor 546 (A-11074), anti-mouse Alexa Fluor 647 (A-S28181), anti-rabbit Alexa Fluor 647 (A-27040), anti-guinea pig Alexa Fluor 647 (A-21450), anti-rat Alexa 555 (A-48263). All primary antibodies were incubated overnight and secondary antibodies were incubated for 2 hours at room temperature. Tissues were mounted in VectaShield (Vector Laboratories, H-1200). For mCherry-Atg8a imaging, tissues were fixed in 4% PFA for 20 minutes and stained with Hoescht before mounting. We imaged samples using a Zeiss LSM 700 confocal microscope equipped with a Plan-Apochromat 63×/1.40 Oil DIC M27 objective at room temperature (22°C) using Zeiss Zen Software and a Nikon A1 HD25 confocal microscope equipped with a CFI Plan Apochromat 60×/1.4 Oil DIC objective at room temperature (22°C) using NIS-Elements Viewer software. Images were deconvoluted using NIS-Elements Viewer software and processed using ImageJ. Co-localization was analyzed by Squassh plugin from Image J [42]. The fraction of the total volume occupied by objects that overlap with objects from the other channel was quantified C(size).

TR-avidin uptake assay and Cathepsin B activity assay—TR-avidin uptake assay and Cathepsin B activity assay were slightly modified according to previous study [43]. For TR-avidin uptake assay, fly intestines 2 hours after pupariation were dissected in Schneider's media and incubated with TR-avidin (80 μg/ml Invitrogen, A820) containing Schneider's media for 20 minutes and chased in 0.5% BSA in cold PBS for 20 minutes and fixed with 4% formaldehyde for 10 minutes. The intestines were briefly washed and mounted with Vectorshield.

For Cathepsin B activity assay, intestines 2 hours after puparium formation were dissected in PBS followed by a 30 minutes incubation in Magic red (1:1000 in PBS, ImmunoChemistry, 937). The intestines were briefly washed and mounted with Vectorshield.

QUANTIFICATION AND STATISTICAL ANALYSIS

Image J (NIH, Bethesda, MD, USA) was used to quantify cell size, puncta, immunofluorescent intensity, co-localization and protein level in western blot results. p values were calculated either using a two-tailed unpaired t test or one-way ANOVA followed by Dunnett's or Bonferroni's multiple comparisons from Graphpad Prism 5 (https://www.graphpad.com/scientific-software/prism/). No animals were excluded from statistical analyses, the experiments were not randomized, and the investigators were not blinded. All error bars are SEM.

Supplementary Material

Refer to Web version on PubMed Central for supplementary material.

ACKNOWLEDGEMENTS

We thank the Baehrecke laboratory, H.J. Bellen, A. Bergmann, G. Chen, H. Gottlinger, G. Juhasz, H. Wang, the Vienna *Drosophila* Resource Center, the Bloomington *Drosophila* stock center, the Kyoto *Drosophila* Genetic Resource Center, and the Electron Microscopy Core Facility at UMass Medical School for advice, flies, antibodies, cell lines and technical support. This work was supported by R35GM131689 to E.H.B. and F30CA239374 to J.L.S.

REFERENCES

1. Fromme JC, Orci L, and Schekman R (2008). Coordination of COPII vesicle trafficking by Sec23. Trends Cell Biol 18, 330–336. [PubMed: 18534853]
2. Zanetti G, Pahuja KB, Studer S, Shim S, and Schekman R (2011). COPII and the regulation of protein sorting in mammals. Nat Cell Biol 14, 20–28. [PubMed: 22193160]
3. Boyadjiev SA, Fromme JC, Ben J, Chong SS, Nauta C, Hur DJ, Zhang G, Hamamoto S, Schekman R, Ravazzola M, et al. (2006). Cranio-lenticulo-sutural dysplasia is caused by a SEC23A mutation leading to abnormal endoplasmic-reticulum-to-Golgi trafficking. Nat Genet 38, 1192–1197. [PubMed: 16980979]
4. Mizushima N, Levine B, Cuervo AM, and Klionsky DJ (2008). Autophagy fights disease through cellular self-digestion. Nature 451, 1069–1075. [PubMed: 18305538]
5. Scott RC, Schuldiner O, and Neufeld TP (2004). Role and regulation of starvation-induced autophagy in the Drosophila fat body. Dev Cell 7, 167–178. [PubMed: 15296714]
6. Kuma A, Hatano M, Matsui M, Yamamoto A, Nakaya H, Yoshimori T, Ohsumi Y, Tokuhisa T, and Mizushima N (2004). The role of autophagy during the early neonatal starvation period. Nature 432, 1032–1036. [PubMed: 15525940]
7. Kihara A, Noda T, Ishihara N, and Ohsumi Y (2001). Two distinct Vps34 phosphatidylinositol 3-kinase complexes function in autophagy and carboxypeptidase Y sorting in Saccharomyces cerevisiae. J Cell Biol 152, 519–530. [PubMed: 11157979]
8. Tooze SA, and Yoshimori T (2010). The origin of the autophagosomal membrane. Nat Cell Biol 12, 831–835. [PubMed: 20811355]
9. Hamasaki M, Furuta N, Matsuda A, Nezu A, Yamamoto A, Fujita N, Oomori H, Noda T, Haraguchi T, Hiraoka Y, et al. (2013). Autophagosomes form at ER-mitochondria contact sites. Nature 495, 389–393. [PubMed: 23455425]
10. Ishihara N, Hamasaki M, Yokota S, Suzuki K, Kamada Y, Kihara A, Yoshimori T, Noda T, and Ohsumi Y (2001). Autophagosome requires specific early Sec proteins for its formation and NSF/SNARE for vacuolar fusion. Mol Biol Cell 12, 3690–3702. [PubMed: 11694599]
11. Shirahama-Noda K, Kira S, Yoshimori T, and Noda T (2013). TRAPPIII is responsible for vesicular transport from early endosomes to Golgi, facilitating Atg9 cycling in autophagy. J Cell Sci 126, 4963–4973. [PubMed: 23986483]

12. Lynch-Day MA, Bhandari D, Menon S, Huang J, Cai H, Bartholomew CR, Brumell JH, Ferro-Novick S, and Klionsky DJ (2010). Trs85 directs a Ypt1 GEF, TRAPPIII, to the phagophore to promote autophagy. Proc Natl Acad Sci U S A 107, 7811–7816. [PubMed: 20375281]
13. Tan D, Cai Y, Wang J, Zhang J, Menon S, Chou HT, Ferro-Novick S, Reinisch KM, and Walz T (2013). The EM structure of the TRAPPIII complex leads to the identification of a requirement for COPII vesicles on the macroautophagy pathway. Proc Natl Acad Sci U S A 110, 19432–19437. [PubMed: 24218626]
14. Behrends C, Sowa ME, Gygi SP, and Harper JW (2010). Network organization of the human autophagy system. Nature 466, 68–76. [PubMed: 20562859]
15. Lamb CA, Nuhlen S, Judith D, Frith D, Snijders AP, Behrends C, and Tooze SA (2016). TBC1D14 regulates autophagy via the TRAPP complex and ATG9 traffic. EMBO J 35, 281–301. [PubMed: 26711178]
16. Ge L, Melville D, Zhang M, and Schekman R (2013). The ER-Golgi intermediate compartment is a key membrane source for the LC3 lipidation step of autophagosome biogenesis. Elife 2, e00947. [PubMed: 23930225]
17. Ge L, Zhang M, and Schekman R (2014). Phosphatidylinositol 3-kinase and COPII generate LC3 lipidation vesicles from the ER-Golgi intermediate compartment. Elife 3, e04135. [PubMed: 25432021]
18. Davis S, Wang J, Zhu M, Stahmer K, Lakshminarayan R, Ghassemian M, Jiang Y, Miller EA, and Ferro-Novick S (2016). Sec24 phosphorylation regulates autophagosome abundance during nutrient deprivation. Elife 5, e21167. [PubMed: 27855785]
19. Lemus L, Ribas JL, Sikorska N, and Goder V (2016). An ER-Localized SNARE Protein Is Exported in Specific COPII Vesicles for Autophagosome Biogenesis. Cell Reports 14, 1710–1722. [PubMed: 26876173]
20. Cui Y, Parashar S, Zahoor M, Needham PG, Mari M, Zhu M, Chen S, Ho HC, Reggiori F, Farhan H, et al. (2019). A COPII subunit acts with an autophagy receptor to target endoplasmic reticulum for degradation. Science 365, 53–60. [PubMed: 31273116]
21. Allen EA, and Baehrecke EH (2020). Autophagy in animal development. Cell Death Differ 27, 903–918. [PubMed: 31988494]
22. Chang TK, Shravage BV, Hayes SD, Powers CM, Simin RT, Wade Harper J, and Baehrecke EH (2013). Uba1 functions in Atg7- and Atg3-independent autophagy. Nat Cell Biol 15, 1067–1078. [PubMed: 23873149]
23. Anding AL, Wang C, Chang TK, Sliter DA, Powers CM, Hofmann K, Youle RJ, and Baehrecke EH (2018). Vps13D Encodes a Ubiquitin-Binding Protein that Is Required for the Regulation of Mitochondrial Size and Clearance. Curr Biol 28, 287–295.e286. [PubMed: 29307555]
24. Shen JL, Fortier TM, Zhao YG, Wang R, Burmeister M, and Baehrecke EH (2021). Vmp1, Vps13D, and Marf/Mfn2 function in a conserved pathway to regulate mitochondria and ER contact in development and disease. Curr Biol.
25. Guillen-Samander A, Leonzino M, Hanna MG, Tang N, Shen H, and De Camilli P (2021). VPS13D bridges the ER to mitochondria and peroxisomes via Miro. J Cell Biol 220.
26. Slagsvold T, Pattni K, Malerod L, and Stenmark H (2006). Endosomal and non-endosomal functions of ESCRT proteins. Trends Cell Biol 16, 317–326. [PubMed: 16716591]
27. Rusten TE, and Stenmark H (2009). How do ESCRT proteins control autophagy? J Cell Sci 122, 2179–2183. [PubMed: 19535733]
28. Takahashi Y, He H, Tang Z, Hattori T, Liu Y, Young MM, Serfass JM, Chen L, Gebru M, Chen C, et al. (2018). An autophagy assay reveals the ESCRT-III component CHMP2A as a regulator of phagophore closure. Nat Commun 9, 2855. [PubMed: 30030437]
29. Christ L, Raiborg C, Wenzel EM, Campsteijn C, and Stenmark H (2017). Cellular Functions and Molecular Mechanisms of the ESCRT Membrane-Scission Machinery. Trends Biochem Sci 42, 42–56. [PubMed: 27669649]
30. Rusten TE, Vaccari T, Lindmo K, Rodahl LM, Nezis IP, Sem-Jacobsen C, Wendler F, Vincent JP, Brech A, Bilder D, et al. (2007). ESCRTs and Fab1 regulate distinct steps of autophagy. Curr Biol 17, 1817–1825. [PubMed: 17935992]

31. Kappeler F, Klopfenstein DRC, Foguet M, Paccaud J-P, and Hauri H-P (1997). The Recycling of ERGIC-53 in the Early Secretory Pathway. Journal of Biological Chemistry 272, 31801–31808.
32. Vietri M, Radulovic M, and Stenmark H (2020). The many functions of ESCRTs. Nat Rev Mol Cell Biol 21, 25–42. [PubMed: 31705132]
33. Juhasz G, Hill JH, Yan Y, Sass M, Baehrecke EH, Backer JM, and Neufeld TP (2008). The class III PI(3)K Vps34 promotes autophagy and endocytosis but not TOR signaling in Drosophila. J Cell Biol 181, 655–666. [PubMed: 18474623]
34. Hurley JH, and Young LN (2017). Mechanisms of Autophagy Initiation. Annu Rev Biochem 86, 225–244. [PubMed: 28301741]
35. Noda T, Kim J, Huang WP, Baba M, Tokunaga C, Ohsumi Y, and Klionsky DJ (2000). Apg9p/Cvt7p is an integral membrane protein required for transport vesicle formation in the Cvt and autophagy pathways. J Cell Biol 148, 465–480. [PubMed: 10662773]
36. Young AR, Chan EY, Hu XW, Kochl R, Crawshaw SG, High S, Hailey DW, Lippincott-Schwartz J, and Tooze SA (2006). Starvation and ULK1-dependent cycling of mammalian Atg9 between the TGN and endosomes. J Cell Sci 119, 3888–3900. [PubMed: 16940348]
37. Ohashi Y, and Munro S (2010). Membrane delivery to the yeast autophagosome from the Golgi-endosomal system. Mol Biol Cell 21, 3998–4008. [PubMed: 20861302]
38. Zhen Y, Spangenberg H, Munson MJ, Brech A, Schink KO, Tan KW, Sorensen V, Wenzel EM, Radulovic M, Engedal N, et al. (2019). ESCRT-mediated phagophore sealing during mitophagy. Autophagy, 1–16.
39. Radulovic M, and Stenmark H (2018). ESCRTs in membrane sealing. Biochem Soc Trans 46, 773–778. [PubMed: 29903934]
40. Davis S, Wang J, and Ferro-Novick S (2017). Crosstalk between the Secretory and Autophagy Pathways Regulates Autophagosome Formation. Dev Cell 41, 23–32. [PubMed: 28399396]
41. Wen JK, Wang YT, Chan CC, Hsieh CW, Liao HM, Hung CC, and Chen GC (2017). Atg9 antagonizes TOR signaling to regulate intestinal cell growth and epithelial homeostasis in Drosophila. Elife 6.
42. Rizk A, Paul G, Incardona P, Bugarski M, Mansouri M, Niemann A, Ziegler U, Berger P, and Sbalzarini IF (2014). Segmentation and quantification of subcellular structures in fluorescence microscopy images using Squassh. Nat Protoc 9, 586–596. [PubMed: 24525752]
43. Allen EA, Amato C, Fortier TM, Velentzas P, Wood W, and Baehrecke EH (2020). A conserved myotubularin-related phosphatase regulates autophagy by maintaining autophagic flux. J Cell Biol 219.

Highlights

- The ESCRT and Vps13D function in a common autophagy pathway
- The ESCRT influences ER maturation and COPII trafficking
- Vps13D influences COPII trafficking
- The ESCRT influences ERGIC and Vps13D availability for Atg9 induction of autophagy

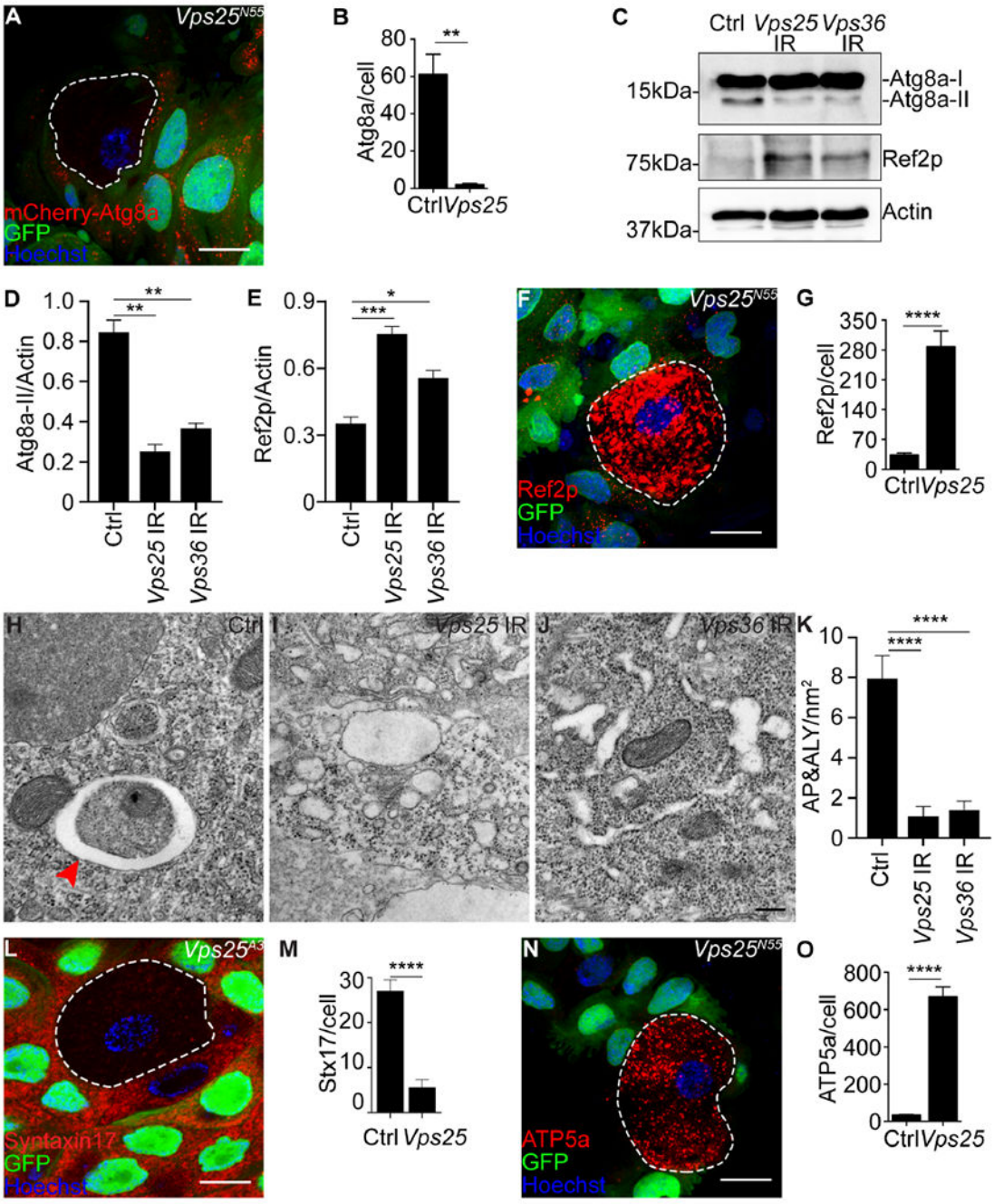

Figure 1. THE ESCRT regulates autophagy in intestine cells.

(A) *Vps25*^{N55} loss-of-function mutant cells (lacking GFP, white dotted line) 2 hours after puparium formation (APF) exhibit decreased mCherry-Atg8a (red) puncta compared to neighboring heterozygous control cells (green).

(B) Quantification of mCherry-Atg8a puncta in *Vps25*(A) mutant cells compared to respective control (Ctrl) cells 2 hours APF. n = 7 (Ctrl), n = 7 (*Vps25*) cells were measured.

(C) Atg8a lipidation is decreased in *Vps25* knockdown intestines expressing *Vps25* RNAi (*Vps25* IR) and *Vps36* knockdown intestines expressing *Vps36* RNAi (*Vps36* IR) compared

to control intestines expressing luciferase RNAi (Ctrl) 2 hours APF. Ref2p/p62 (Ref2p) is increased in both *Vps25* and *Vps36* knockdown intestines compared to control intestines.
(D) Quantification of the ratio of Atg8a-II/Actin in *Vps25* and *Vps36* knockdown intestines compared to control intestines.
(E) Quantification of the ratio of Ref2p/Actin in *Vps25* and *Vps36* knockdown intestines compared to control intestines. Error bars are SEM. *, p<0.05, **, p.<0.005, ***, p<0.0005. Representative of 3 more independent biological experiments.
(F) $Vps25^{N55}$ mutant cells (lacking GFP, white dotted line) possess increased Ref2p/p62 puncta (red) compared to neighboring control cells (green).
(G) Quantification of Ref2p/p62 puncta in *Vps25*(L) mutant cells compared to control cells 2 hours APF. n = 6 (Ctrl), n = 7 (*Vps25*) cells were measured.
(H-J) TEM images reveal decreased autophagosomes and autolysosomes (red arrowheads) in cells from intestines expressing *Vps25* RNAi (*Vps25* IR) and *Vps36* RNAi (*Vps36* IR) compared to control cells from intestines expressing luciferase RNAi (Ctrl).
(K) Quantification of autophagosome (AP) and autolysosome (ALY) structures in TEM of control (Ctrl), *Vps25* knockdown (*Vps25* IR) and *Vps36* knockdown (*Vps36* IR) intestines 2 hours after puparium formation (APF). n=16 (Ctrl), n=11 (Vps25), n (Vps36)=12 TEM images were analyzed.
(L) $Vps25P^{A3}$ loss-of-function mutant cell clones (lacking GFP, white dotted line) two hours APF possess decreased Syntaxin17 (red) puncta compared to neighboring control cells.
(M) Quantification of Syntaxin17 puncta in *Vps25* mutant cells compared to control cells. n=9 (Ctrl), n=11 (*Vps25*) cells were measured.
(N) $Vps25^{N55}$ mutant cells (lacking GFP, white dotted line) possess increased ATP5a puncta (red) compared to neighboring control cells (green) in intestines 2 hours APF.
(O) Quantification of ATP5a puncta in *Vps25*(N) mutant cells compared to control cells 2 hours APF. n = 6 (Ctrl), n = 6 (*Vps25*) cells were measured.
Scale bars represent 20 μm and scale bars in TEM represent 200 nm. Data are presented as mean ± SEM. *, p<0.05, **, p<0.005, ***, p<0.0005, ****, p<0.0001, from unpaired, two-tailed t-test. Representative of 3 or more independent biological experiments. See also Figure S1.

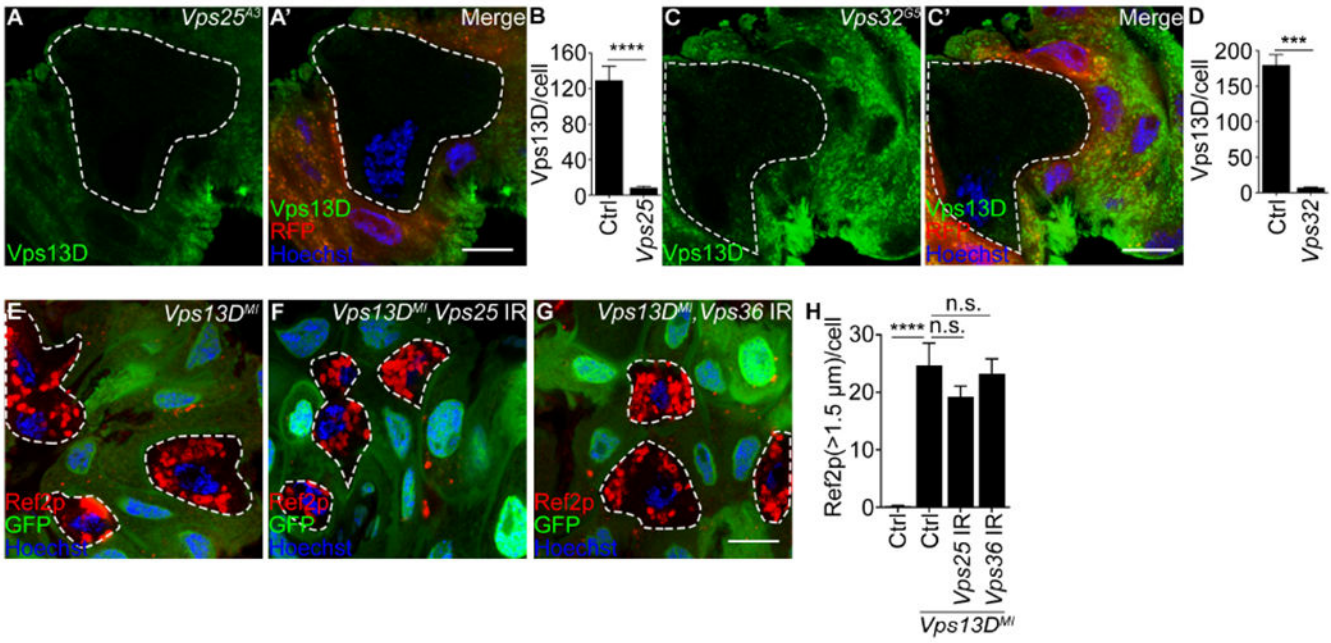

Figure 2. The ESCRTs and Vps13D influence autophagy in a similar manner.

(A-A') *Vps25*^{A3} loss-of-function mutant cells (lacking RFP, white dotted line) 2 hours APF possess decreased Vps13D puncta (green) compared to neighboring control cells (red).

(B) Quantification of Vps13D puncta in *Vps25*(A) mutant cells compared to neighboring control cells, n = 6 (Ctrl), n = 6 (*Vps25*) cells were measured.

(C-C') *Vps32*^{G5} loss-of-function mutant cells (lacking RFP, white dotted line) 2 hours APF possess decreased Vps13D puncta (green) compared to neighboring control cells (red).

(D) Quantification of Vps13D puncta in *Vps32* (C) mutant cells compared to neighboring control cells 2 hours APF. n = 6 (Ctrl), n = 7 (*Vps32*) cells were measured.

(E-G) *Vps13D*^{MI} loss-of-function mutant cells in either *Vps25* RNAi (F) or *Vps36* RNAi (G) expressing intestines possess similar cell size and Ref2p/p62 puncta levels compared to *Vps13D*^{MI} single mutant cells expressing luciferase RNAi (E) 2 hours APF.

(H) Quantification of Ref2p/p62 puncta of *Vps13D* (E), *Vps13D*^{MI}, *Vps25RNAi* (F) and *Vps13D*^{MI}, *Vps36* RNAi (G) mutant cells 2 hours APF. n = 6 (*Vps13D*^{MI}), n = 7 (*Vps13D*^{MI}, *Vps25* RNAi), n = 7 (*Vps13D*^{MI}, *Vps36* RNAi) cells were measured.

Scale bars represent 20 μm. Data are presented as mean ± SEM. n.s. = not significant, ***, p<0.0005, ****, p<0.0001 from unpaired, two-tailed t-test and data in (H) was calculated by one-way ANOVA followed by Dunnett's multiple comparisons. Representative of 3 or more independent biological experiments.

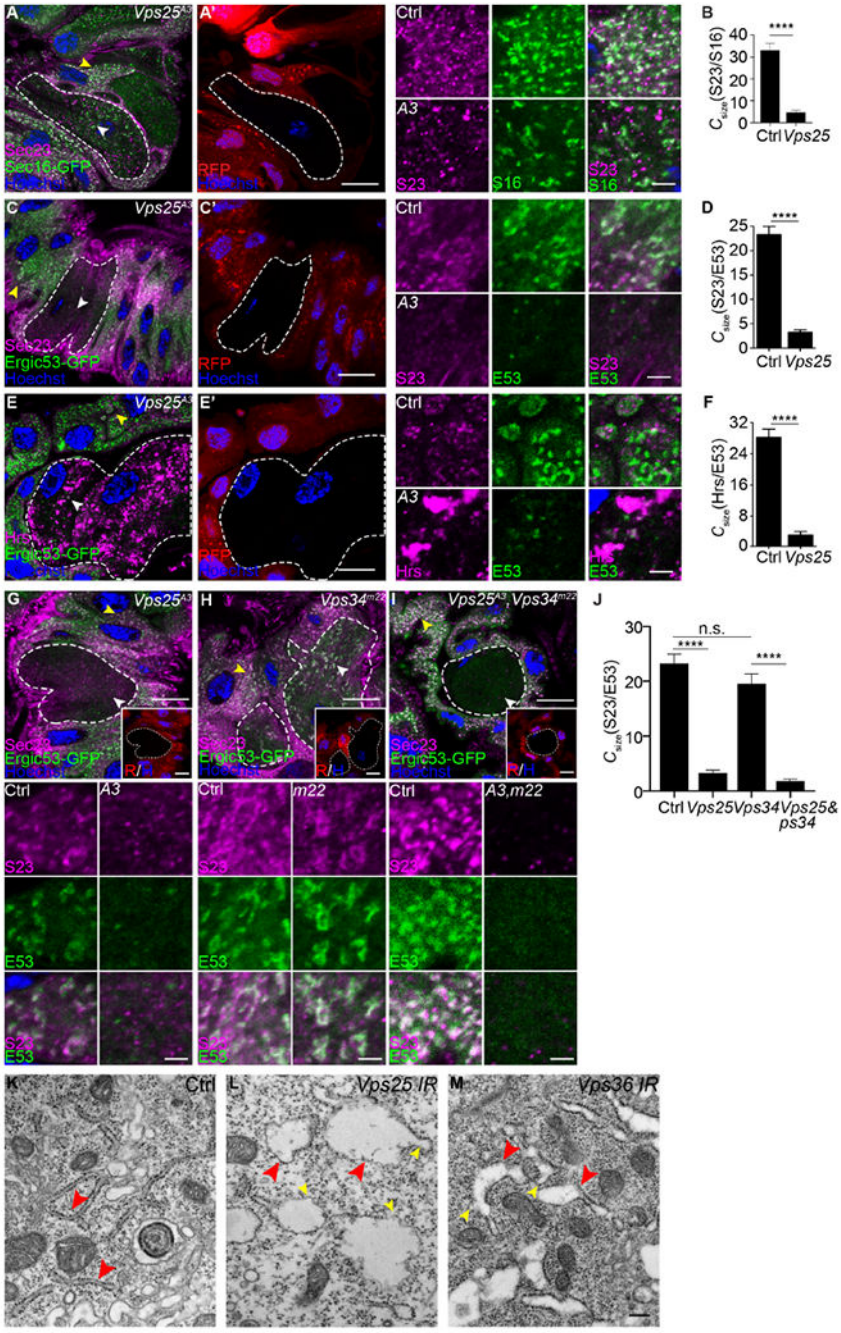

Figure 3. The ESCRT influences markers of COPII vesicle trafficking.

(A-A') *Vps25*^{A3} loss-of-function mutant intestine cell clones (lacking RFP, white dotted line) possess comparable Sec16 (Sec16-GFP, green) puncta to neighboring control cells. *Vps25* mutant cells exhibit decreased Sec23 and Sec16 co-localization compared to control cells.

(B) Quantification of Sec23 and Sec16 co-localization (C_{size}) in *Vps25*^{A3} mutant cells compared to control cells, n = 10 (Ctrl), n = 5 (*Vps25*) animal midguts were measured.

(C-C') *Vps25P*^{A3} loss-of-function mutant cells (lacking RFP, dotted white line) exhibit decreased Sec23 (magenta) and Ergic53-GFP (green) puncta compared to neighboring control cells (red) 2 hours APF. Hrs and Ergic53 co-localization is also decreased in *Vps25*^{A3} mutant cells.

(D) Quantification of Sec23 (S23) and Ergic53 (E53) co-localization (C_{size}) in *Vps25*^{A3} mutant cells compared to control cells 2 hours APF. n = 6 (Ctrl), n = 7 (*Vps25*) cells were measured.

(E-E') *Vps25*^{A3} mutant cells (lacking RFP, dotted white line) possess increased Hrs puncta (magenta) and decreased Ergic53 puncta compared to neighboring control cells (red) 2 hours APF. Hrs and Ergic53 co-localization is also decreased in *Vps25*^{A3} mutant cells.

(F) Quantification of Hrs (Hrs) and Ergic53 (E53) co-localization in *Vps25* mutant cells compared to control cells 2 hours APF. n = 7 (Ctrl), n = 7 (*Vps25*) cells were measured.

(G) *Vps25*^{A3} loss-of-function mutant cells (lacking RFP, white dotted line) 2 hours APF possess decreased Sec23 (Sec23, magenta) and Ergic53 (Erigc53-GFP, green) puncta compared to neighboring control cells. Sec23 and Ergic53 co-localization is also decreased in *Vps25*^{A3} mutant cells. The absence of DNA stain in the *Vps25* mutant cell is because the nucleus is out of the focal plane.

(H) *Vps34*^{m22} loss-of-function mutant cells (lacking RFP, white dotted line) 2 hours APF possess comparable Sec23 and Ergic53 puncta to neighboring control cells. Sec23 and Ergic53 co-localization is not influenced in *Vps34*^{m22} mutant cells.

(I) *Vps25*^{A3}, *Vps34*^{m22} loss-of-function double mutant cells (lacking RFP, whit dotted line) 2 hours APF possess decreased Sec23 and Ergic53 puncta compared to neighboring control cells. Sec23 and Ergic53 co-localization is decreased in *Vps25*^{A3}, *Vps34*^{m22} double mutant cells. The absence of DNA stain in the double mutant cell is because the nucleus is out of the focal plane.

(J) Quantification of Sec23 (S23) and Ergic53 (E53) co-localization (C_{size}) in *Vps25*^{A3} (G), *Vps34*^{m22} (H) and *Vps25*^{A3}, *Vps34*^{m22} (I) mutant cells compared to neighboring control cells, n =10 (Ctrl), n =9 (*Vps25*), n =8 (*Vps34*), n=9 (*Vps25*, *Vps34*) cells were measured.

(K-M) TEM images reveal dilated ER in cells from intestines expressing either *Vps25* RNAi (L, *Vps25* IR) or *Vps36* RNAi (M, *Vps36* IR) compared to the cells of control intestines expressing luciferase RNAi (K, Ctrl) 2 hours APF. Red arrowheads indicate rough ER, and yellow arrowheads indicate abnormal tubular projections on ER surface.

Insets of mutant cells from lower magnification images as indicated by white arrowheads, and insets of control cells are indicated by yellow arrowheads in lower magnification images. Scale bars in lower magnification represent 20 μm, and scale bars in insets represent 2.5 μm. Scale bar of TEM images represent 200 nm. Data are presented as mean ± SEM. ****, p<0.0001 from unpaired, two-tailed t-test. Representative of 3 or more independent biological experiments. See also Figures S2–S4.

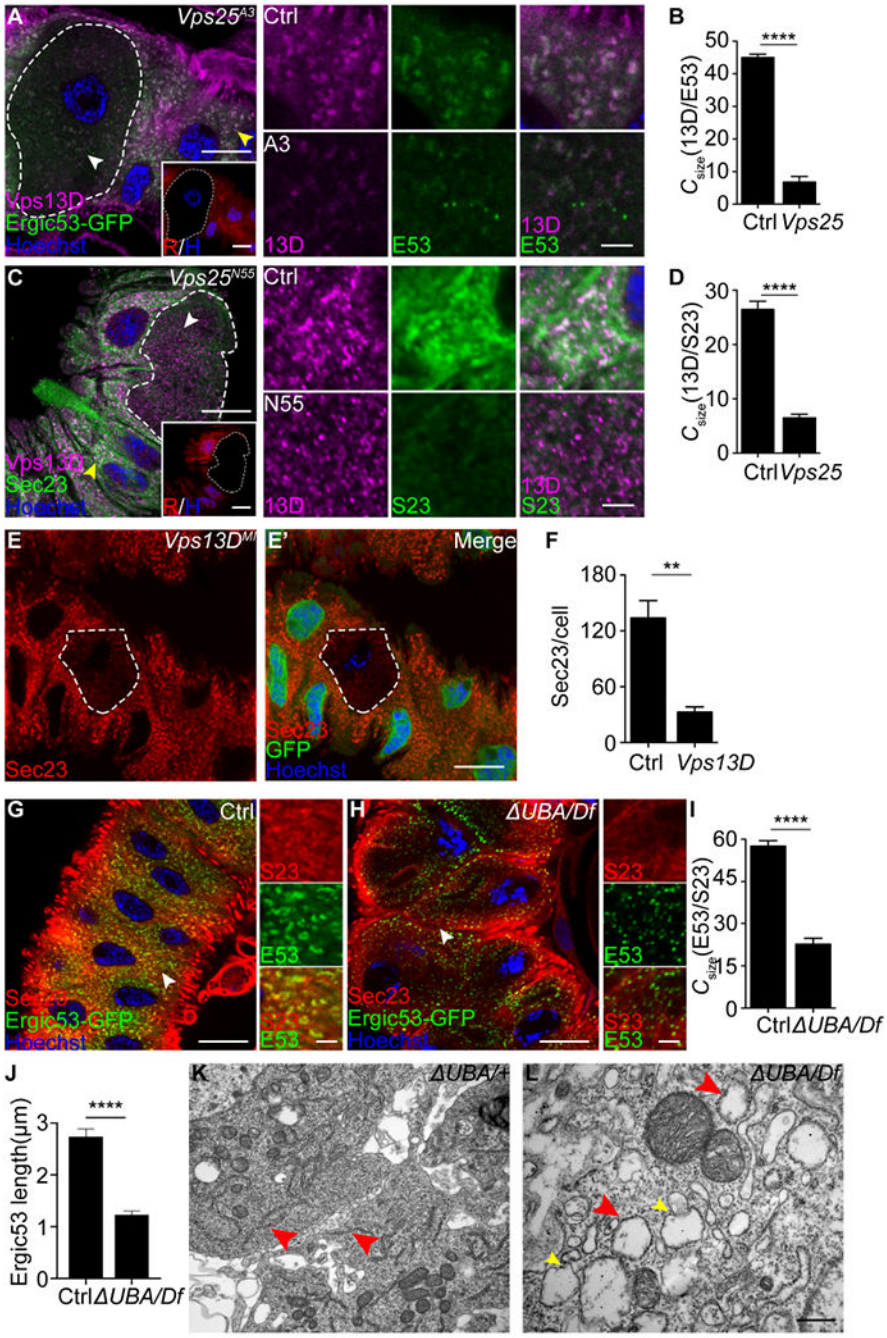

Figure 4. Vps13D, COPII and the ERGIC appear to function in a common pathway.

(A) *Vps25*^{A3} mutant cells (lacking RFP (R, right bottom Conner, H represent Hoechst), dotted white line) possess decreased Vps13D puncta (magenta) and Ergic53 puncta compared to neighboring control cells (red) 2 hours APF. Vps13D and Ergic53 co-localization is also decreased in *Vps25*^{A3} mutant cells.

(B) Quantification of Vps13D (13D) and Ergic53 (E53) co-localization in *Vps25* mutant cells compared to control cells 2 hours APF. n = 8 (Ctrl), n = 8 (*Vps25*) cells were measured.

(C) *Vps25*^{N55} loss-of-function mutant cells (lacking RFP (R, right bottom Conner, H represent Hoechst), white dotted line) exhibit decreased level of Vps13D (magenta) and Sec23 (green) puncta compared to neighboring control cells (red) 2 hours APF. Vps13D co-localization with Sec23 is decreased in *Vps25* mutant intestine cells. The absence of DNA stain in the *Vps25* mutant cell is because the nucleus is out of the focal plane.
(D) Quantification of Vps13D (13D) and Sec23 (S23) co-localization (C_{size}) in *Vps25* mutant cells compared to control cells 2 hours APF. n = 7 (Ctrl), n = 8 (*Vps25*) cells were measured per midgut. Insets of control and mutant cells (A, C) are from lower magnification images indicated by yellow and white arrowheads.
(E-E') *Vps13D*^{MI} loss-of-function mutant intestine cells (lacking GFP, white dotted line) possess decreased Sec23 puncta (red) compared to neighboring control cells (green) 2 hours APF.
(F) Quantification of Sec23 puncta in *Vps13D* mutant cells compared to neighboring control cells 2 hours APF. n = 10 (Ctrl), n = 8 (*Vps13D*) cells were measured.
(G-H) Ergic53-GFP (green) expressing intestines from control *w*^{1118} (G, Ctrl), and *Vps13D ΔUBA/Df(3L)BSC613* (H, *ΔUBA/Df*) pupae 2 hours APF were dissected. The intestines were stained with antibody against Sec23 (red). Co-localization of Sec23 and Ergic53 is decreased in *Vps13D* (*ΔUBA/Df)* intestines compared to control intestines. Insets in (G-H) are from lower magnification images indicated by arrowheads.
(I) Quantification of colocalization of Sec23 (S23) and Ergic53 (E53) in control (Ctrl) and *Vps13D* (*ΔUBA/Df*) intestine cells 2 hours APE n = 9 (Ctrl), n = 12 (*ΔUBA/Df*) animal midguts were measured.
(J) Quantification of Ergic53 puncta length in control (Ctrl) and mutant (*ΔUBA/Df*) cells. n = 31 (Ctrl), n = 41 (*ΔUBA/Df*) puncta were measured.
(K-L) TEM images reveal dilated ER in cells from *Vps13D* (*ΔUBA/Df*) intestines (L) compared to the cells of control (K, *ΔUBA*/+) 2 hours APF. Red arrowheads indicate rough ER, and yellow arrowheads indicate abnormal tubular projections on ER surface.
Scale bars in lower magnification images represent 20 μm, and scale bars in insets represent 2.5 μm. Scale bar in TEM represents 200 nm. Data are presented as mean ± SEM. **, $p<0.005$, ****, $p<0.0001$ from unpaired, two-tailed t-test. Representative of 3 or more independent biological experiments. See also Figure S5.

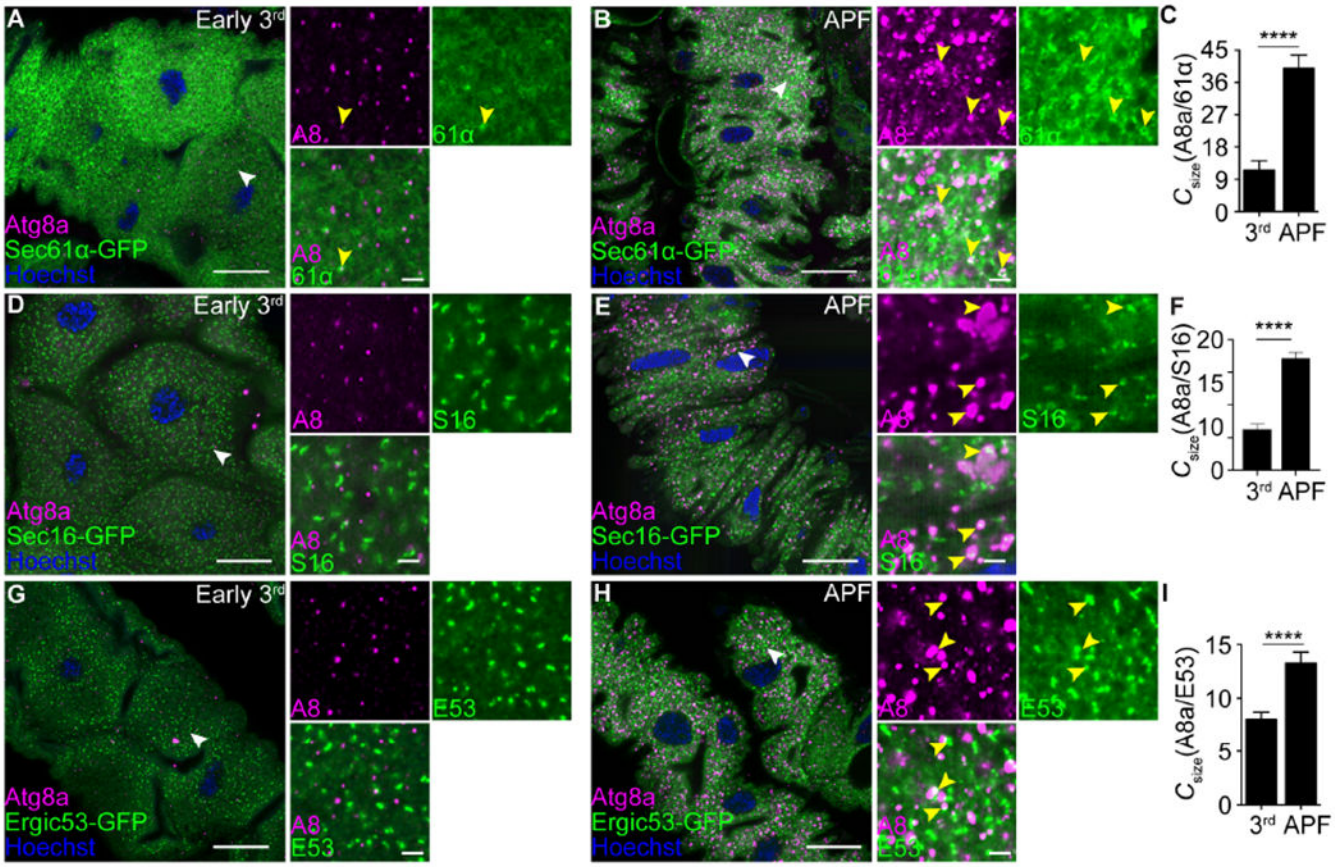

Figure 5. Atg8a localization with the ERGIC increases during autophagy.

(A-B) Intestines isolated from early 3rd instar larvae (3rd) and 2 hours APF expressing Sec61α-GFP were stained with antibody against Atg8a. Co-localization (C_{size}) of Atg8a (magenta, A8) and Sec61α (green, S61a) was increased in intestines 2 hours APF (B) compared to early 3rd larval instar intestines (A).

(C) Quantification of Atg8a and Sec61α co-localization in early 3rd larval instar intestines and 2 hours APF intestines, n = 11 (3rd), n = 12 (APF) animal midguts were measured.

(D-E) Intestines isolated from early 3rd instar larvae (3rd) and 2 hours APF expressing Sec16-GFP were stained with antibody against Atg8a. Co-localization (C_{size}) of Atg8a (magenta, A8) and Sec16 (green, S16) was increased in intestines 2 hours APF (E) compared to early 3rd larval instar intestines (D).

(F) Quantification of Atg8a and Sec16 co-localization in early 3rd larval instar intestines and 2 hours APF intestines. n = 11 (3rd), n = 12 (APF) animal midguts were measured.

(G-H) Intestines isolated from early 3rd instar larvae and 2 hours APF expressing Ergic53-GFP were stained with antibody against Atg8a. Co-localization of Atg8a (magenta) and Ergic53 (green) was increased in intestines 2 hours APF (H) compared to early 3rd larval instar intestines (G).

(I) Quantification of Atg8a and Ergic53 co-localization in early 3rd larval instar intestines and 2 hours APF intestines. n = 12 (3rd), n = 12 (APF) animal midguts were measured.

Scale bars in lower magnification represent 20 μm and scale bars in insets represent 1 μm. Insets are from the lower magnification images as indicated by the white arrowheads. Yellow arrowheads in insets indicate colocalized puncta.

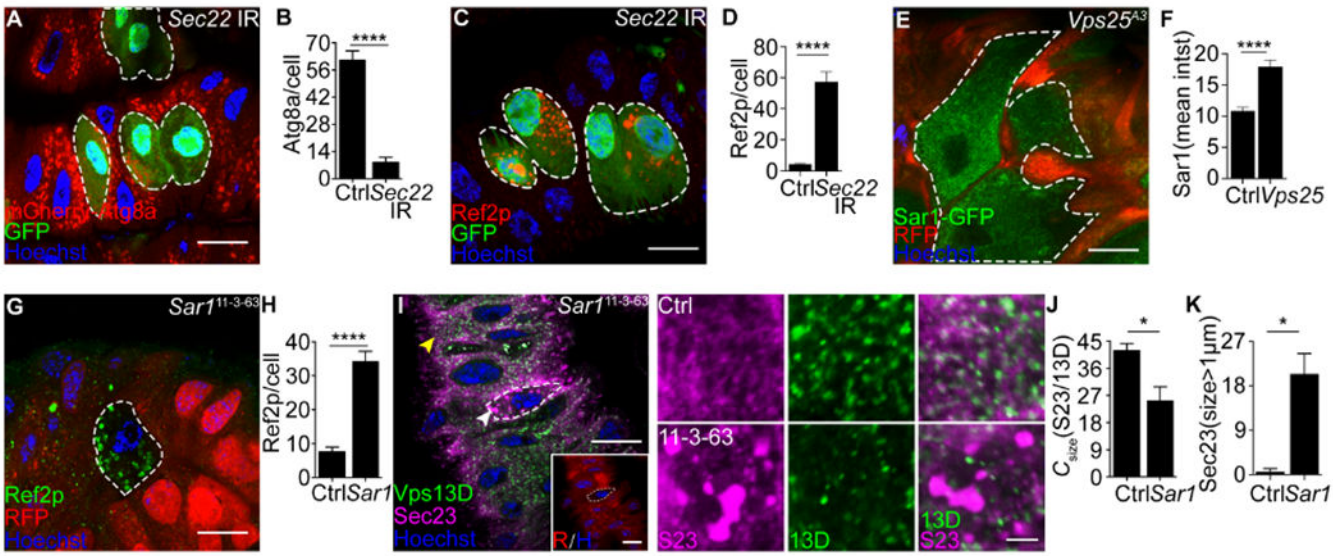

Figure 6. COPII is required for autophagy.

(A) Cells expressing *Sec22* RNAi from intestines (green) exhibit decreased mCherry-Atg8a puncta formation compared to neighboring control intestine cells (non-green) 2 hours APF.

(B) Quantification of Atg8a puncta in $Sec22^{IR}$ cells compared to control intestine cells 2 hours APF. n = 8 (Ctrl), n = 8 ($Sec22^{IR}$) cells were measured.

(C) *Sec22* knockdown clone cells (green cells, white dotted line) exhibit increased Ref2p/p62 puncta (red) compared to neighboring control cells 2 hours APF.

(D) Quantification of Ref2p/p62 puncta in *Sec22* knockdown cells compared to control cells. n=10 (*Ctrl*), n=10 (*Sec22*) cells were measured.

(E) $Vps25P^{A3}$ loss-of-function mutant cells (lacking GFP, white dotted line) 2 hours APF possess increased Sar1 (Sar1-GFP, green) compared to neighboring control cells.

(F) Quantification of Sar1 intensity in *Vps25* mutant cells compared to control cells. n=6 (Ctrl), n=6 (*Vps25*) cells were measured.

(G) $Sar1^{11\text{-}3\text{-}63}$ loss-of-function mutant cells (lacking RFP, white dotted line) possess increased Ref2p/p62 puncta (green) compared to neighboring control cells (red) 2 hours APF.

(H) Quantification of Ref2p/p62 puncta in $Sar1^{11\text{-}3\text{-}63}$ mutant cells compared to control cells 2 hours APF. n = 7 (Ctrl), n = 7 (*Sar1*) cells were measured.

(I) $Sar1^{11\text{-}3\text{-}63}$ mutant cells (lacking RFP, white dotted line) possess decreased Vps13D puncta (green) and enlarged Sec23 puncta (magenta) compared to neighboring control cells (red) 2 hours APF. Sec23 and Vps13D co-localization is decreased in $Sar1^{11\text{-}3\text{-}63}$ mutant cells.

(J) Quantification of Vps13D and Sec23 co-localization in $Sar1^{11\text{-}3\text{-}63}$ mutant cells 2 hours APF compared to control cells. n = 6 (Ctrl), n = 6 (*Sar1*) cells were measured.

(K) Quantification of Sec23 puncta larger than 1 μm in $Sar1^{11\text{-}3\text{-}63}$ mutant cells 2 hours APF compared to control cells. n = 6 (Ctrl), n = 6 (*Sar1*) cells were measured. Insets of $Sar1^{11\text{-}3\text{-}63}$ mutant cells are from lower magnification images as indicated by white arrowheads, and insets of control cells (Ctrl) are indicated by yellow arrowheads in lower magnification images.

Scale bars in lower magnification represent 20 μm and scale bar in inset represents 2.5 μm. Data are presented as mean ± SEM. *, $p<0.05$, ****, $p<0.0001$ from unpaired, two-tailed t-test. Representative of 3 or more independent biological experiments.

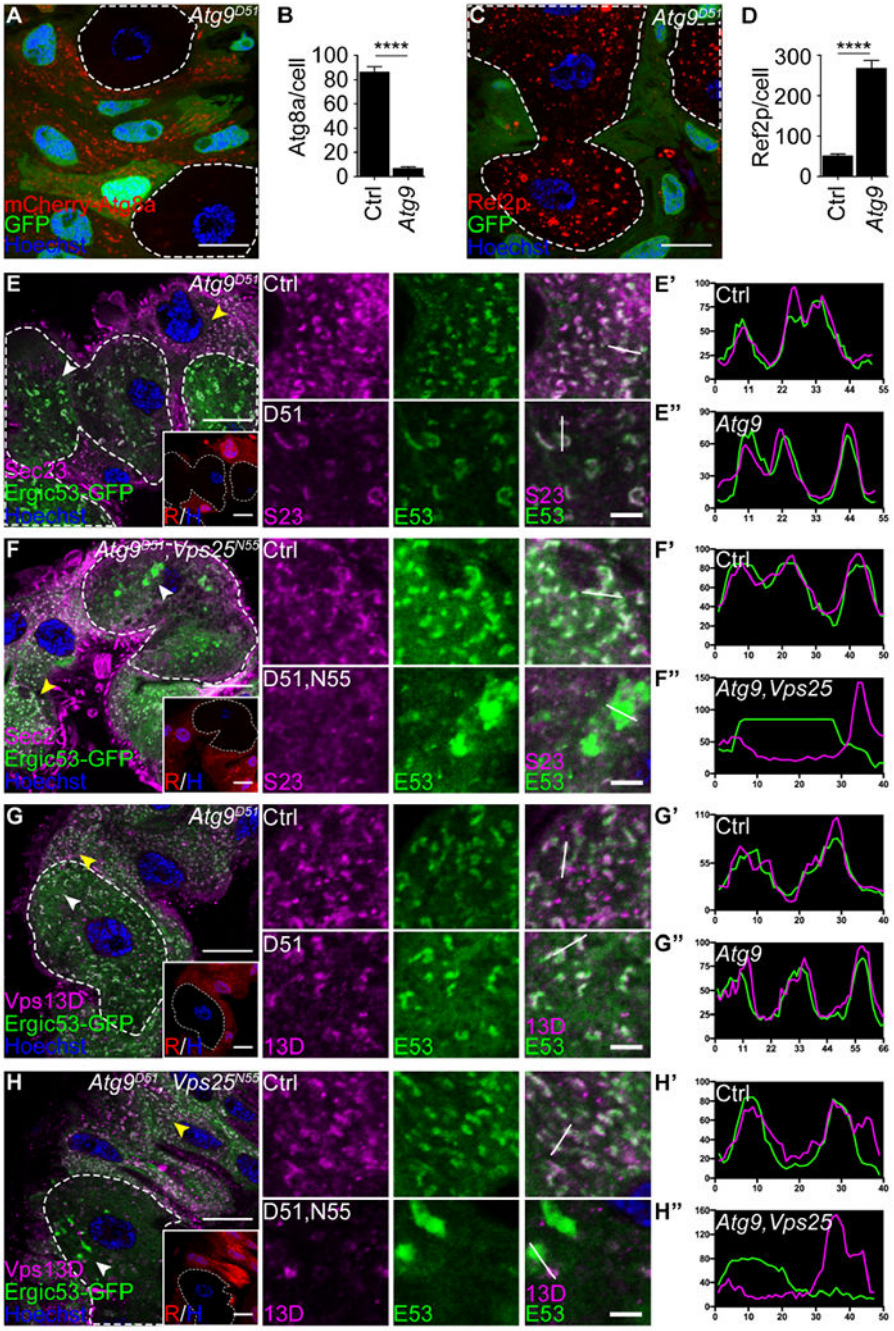

Figure 7. ESCRT-regulated COPII trafficking is required for Atg9-dependent autophagy.

(A) *Atg9*^{D51} loss-of-function mutant intestine cells (lacking GFP, white dotted line) 2 hours APF exhibit decreased mCherry-Atg8a (red) puncta formation compared to neighboring control cells (green)

(B) Quantification of mCherry-Atg8a puncta in *Atg9* mutant cells compared to control cells. n = 10 (Ctrl), n = 10 (*Atg9*) cells were measured.

(C) *Atg9*^{D51} mutant cells (lacking GFP, white dotted line) possess increased Ref2p/p62 (red) puncta compared to neighboring control cells (green) 2 hours APF.

(D) Quantification of Ref2p/p62 puncta in *Atg9* mutant cells 2 hours APF compared to control cells. n =11 (Ctrl), n =11 (*Atg9*) cells were measured.
(E) $Atg9^{D51}$ mutant cells (lacking RFP, white dotted line) exhibit elongated Sec23 (magenta) and Ergic53-GFP (green) puncta compared to neighboring control cells (red) 2 hours APF. Sec23 and Ergic53 association is comparable in both control cells and *Atg9* mutant cells.
(E'-E") Plot analyses of Sec23 and Ergic53 co-localization in *Atg9* mutant intestine cells and control intestine cells. Signals on the white line were analyzed (Insets).
(F) $Atg9^{D51}$, $Vps25^{N55}$ double mutant intestine cells (lacking RFP, white dotted line) exhibit decreased Sec23 (magenta) and Ergic53 (green) puncta compared to neighboring control cells (red) 2 hours APF. Sec23 dissociates from Ergic53 in *Atg9* and *Vps25* double mutant intestine cells compared to control cells 2 hours after pupation.
(F'-F") Plot analyses of Sec23 and Ergic53 co-localization in *Atg9* and *Vps25* double mutant intestine cells and control intestine cells. Signals on the white line were analyzed (Insets).
(G) $Atg9^{D51}$ mutant intestine cells (lacking RFP, white dotted line) exhibit elongated Vps13D (magenta) and Ergic53 (green) puncta compared to neighboring control cells (red) 2 hours APF. Vps13D and Ergic53 association is comparable in both control cells and *Atg9* mutant cells.
(G'-G") Plot analyses of Vps13D and Ergic53 co-localization in *Atg9* mutant intestine cells and control intestine cells. Signals on the white line were analyzed (Insets).
(H) $Atg9^{D51}$, $Vps25^{N55}$ double mutant intestine cells (lacking RFP, white dotted line) exhibit decreased Vps13D (magenta) and ERGIC53 (green) puncta compared to neighboring control cells (red) 2 hours APF. Vps13D dissociates from Ergic53 in *Atg9* and *Vps25* double mutant cells compared to control cells.
(H'-H") Plot analyses of Vps13D and Ergic53 co-localization in $Atg9^{D51}$, $Vps25^{N55}$ double mutant intestine cells and control intestine cells. Signals on the white line were analyzed (Insets).
Scale bars in lower magnification represent 20 μm, and scale bars in insets represent 2.5 μm. Inset of mutant cells (E-H) are from lower magnification images as indicated by white arrowheads, and insets of control cells (Ctrl) are indicated by yellow arrowheads in lower magnification images. Data are presented as mean ± SEM. ****, $p<0.0001$ from unpaired, two-tailed t-test. Representative of 3 or more independent biological experiments. See also Figure S6.

KEY RESOURCES TABLE

REAGENT or RESOURCE	SOURCE	IDENTIFIER
Antibodies		
Vps13D	Eric Baehrecke	This study
Ref2p/p62	Gabor Juhasz	N/A
Hrs	Hugo J. Bellen	N/A
Atg8a	Cell Signaling	13733
Sec23	Thermo Fisher	PA1-069A
GM130	Abcam	AB30637
ATP5a	Abcam	Ab14748
Syntaxin 17	Gabor Juhasz	N/A
Atg9A	Novus Biologicals	NB110-56893SS
Actin	Developmental Studies Hybridoma Bank	JLA20
Ergic53	Sigma-Aldrich	E1031
Calnexin	Proteintech	10427-2-AP
LAMP2	Developmental Studies Hybridoma Bank	H4B4
Anti-mouse Alexa Fluor 488	Invitrogen	A-11029
Anti-rabbit Alexa Fluor 488	Invitrogen	A-27034
Anti-rabbit Alexa Fluor 546	Invitrogen	A-11035
Anti-mouse Alexa Fluor 546	Invitrogen	A-11030
Anti-guinea pig Alexa Fluor 546	Invitrogen	A-11074
Anti-mouse Alexa Fluor 647	Invitrogen	A-S28181
Anti-rabbit Alexa Fluor 647	Invitrogen	A-27040
Anti-guinea pig Alexa Fluor 647	Invitrogen	A-21450
Chemicals		
TR-avidin	Invitrogen	A820
Magic red	ImmunoChemistry	937
PBS	GIBCO	70011
Hoechst	Invitrogen	33342
Paraformaldehdye	Electron Microscopy Sciences	15710
Triton X-100	Sigma	T8787
Heptane	Sigma	34873
Methanol	Sigma	34860
Vectashield	Vector Laboratories	H-1200
Tris-HCl	Sigma	T3253
NaCl	Fisher	BP358-212
Normal goat serum	Life technologies	PCN5000
EDTA	Quality Biological	321-027-101

REAGENT or RESOURCE	SOURCE	IDENTIFIER
Schneider's media	Thermo Fisher Scientific	21720024
Experimental models: Organisms/strains		
y w hsFlp; pmCherry-Atg8a; Act>CD2>GAL4, UAS-nlsGFP	Eric Baehrecke	N/A
y w hsFlp; FRT42D,Ubi-nlsGFP; pmCherry-Atg8a	Eric Baehrecke	N/A
y w hsFlp; Ubi-nlsGFP, FRT40A; pmCherry-Atg8a	Eric Baehrecke	N/A
y w hsFlp; pmCherry-Atg8a;FRT82B, Ubi-nlsGFP	Eric Baehrecke	N/A
y w hsFlp; FRT42D,Ubi-nlsGFP	Eric Baehrecke	N/A
y w hsFlp; FRT42D,Ubi-nlsRFP	Eric Baehrecke	N/A
y w hsFlp; Ubi-nlsGFP, FRT40A	Eric Baehrecke	N/A
y w hsFlp; If/CyO; FRT82B, Ubi-nlsRFP	Eric Baehrecke	N/A
y w hsFlp; If/CyO; Ubi-nlsGFP FRT2A	Eric Baehrecke	N/A
CG32113^{MI11101}	Bloomington *Drosophila* stock center	56282
Df(3L)BSC631	Bloomington *Drosophila* stock center	25722
w^{1118}	Eric Baehrecke	N/A
pmCherry-Atg8a	Eric Baehrecke	N/A
NP1-Gal4	Eric Baehrecke	N/A
UAS-GalT-GFP	Eric Baehrecke	Eric Baehrecke
Ergic53-GFP	Vienna *Drosophila* RNAi Center (VDRC)	318063
Sec61α-GFP	Vienna *Drosophila* RNAi Center (VDRC)	318343
Sec22-GFP	Vienna *Drosophila* RNAi Center (VDRC)	318332
Sec16-GFP	Vienna *Drosophila* RNAi Center (VDRC)	318329
Sar1-GFP	Eric Baehrecke	This study
YFP-Rab7	Bloomington *Drosophila* stock center	62545
Hrs^{D28},FRT40A/CyO, tb	Bloomington *Drosophila* stock center	54574
FRT42D, Vps25^{N55}/CyO, tb	Andreas Bergmann	N/A
FRT42D, Vps25^{A3}/CyO, tb	Bloomington *Drosophila* stock center	39633
FRT42D, Vps32^{G5}/CyO, tb	Bloomington *Drosophila* stock center	39635
FRT42D, Atg9^{D51}/CyO, tb	Guangchao Chen	N/A
FRT42D, Vps34^{m22}/CyO, tb	Thomas P. Neufeld	N/A
FRT82B, Vps22^{SS6}/TM6B,tb	Bloomington *Drosophila* stock center	39631
FRT82B, Sar1$^{11-3-63}$/TM6B, tb	Bloomington *Drosophila* stock center	53710
UAS-Sec22 IR	Bloomington *Drosophila* stock center	34893
Deposited data		
Original western blot results	This study; Mendeley Data	DOI: 10.17632/6wj3s6d4by.1

REAGENT or RESOURCE	SOURCE	IDENTIFIER
Software and algorithms		
Image J	NIH	https://imagej.nih.gov/ij/
Prism	Graphpad Software	https://www.graphpad.com/scientific-software/prism/
ZEN	Zeiss	https://www.zeiss.com/microscopy/us/products/microscopesoftware/zen.html
NIS-Elements	Nikon	https://www.microscope.healthcare.nikon.com/products/software/nis-elements
Biorender	Biorender	https://biorender.com/